With an observed detection every 20 days, the F ring appears to be the solar system's most sensitive detector of meteoroids in the 10-cm size range. Given the number of rings known, this may seem surprising. Several ring properties work together to make this so. First, the F ring is both narrow and optically thin, so an injection of a few cubic meters of dust is an observable event. A similar amount of material injected into a broader but faint ring such as the C ring or Cassini division would pass unnoticed. Second, with typical optical depths of ~0.1, the ring is optically thick enough to represent a substantial target for impactors; most analogous rings, such as Saturn's E and G rings, are fainter by many orders of magnitude. Third, because the ring is narrow, an ejected dust grain is less likely to recollide with a large particle during each passage through the ring plane; as a result, the lifetime of a burst event is enhanced. In reality, narrow ringlets embedded in the Maxwell and Titan gaps of the C ring may serve as comparable detectors but were not as well observed by Voyager.

The flux of meteoroids has importance for the formation of the ring systems and the lifetimes of satellites. Results for the F ring raise the possibility that, by better calibrating our "detector," we could place new and important constraints on the flux of meteoroids in this intermediate size range. Further observations by the Hubble Space Telescope or the Cassini Orbiter should make this possible. Furthermore, a closer look at the F ring should reveal the more frequent, smaller bursts that were presumably overlooked in this analysis, possibly yielding the slope of meteoroid influx throughout the 1- to 100-cm range. It may also be possible to detect an asymmetry in the longitudes where bursts originate, as would be predicted by some models of meteoroid bombardment (*20*); this asymmetry, in turn, could shed light on whether the projectiles are approaching Saturn on cometary or Centaur-like orbits, with implications for their dynamical origin.

References and Notes

1. T. Gehrels *et al.*, *Science* **207**, 434 (1980).
2. B. A. Smith *et al.*, *ibid.* **212**, 163 (1981).
3. B. A. Smith *et al.*, *ibid.* **215**, 504 (1982).
4. S. F. Dermott, *Nature* **290**, 454 (1981).
5. M. R. Showalter and J. A. Burns, *Icarus* **52**, 526 (1982).
6. R. A. Kolvoord, J. A. Burns, M. R. Showalter, *Nature* **345**, 695 (1990).
7. M. R. Showalter, J. B. Pollack, M. E. Ockert, L. Doyle, J. B. Dalton, *Icarus* **100**, 394 (1992).
8. J. A. Burns, M. R. Showalter, G. Morfill, in *Planetary Rings*, R. Greenberg and A. Brahic, Eds. (Univ. of Arizona Press, Tucson, AZ, 1984), pp. 200–272.
9. A. S. Bosh and A. S. Rivkin, *Science* **272**, 518 (1996).
10. P. D. Nicholson *et al.*, *ibid.*, p. 509.
11. C. Roddier *et al.*, *IAU Circular 6515* (1996).
12. M. R. Showalter, *Bull. Am. Astron. Soc.* **26**, 1150 (1994).
13. S. P. Synnott, R. J. Terrile, R. A. Jacobson, B. A. Smith, *Icarus* **53**, 156 (1983).
14. Intervals were 1 to 12 days, depending on image availability.
15. M. R. Showalter, *Bull. Am. Astron. Soc.* **29**, 999 (1997).
16. J. N. Cuzzi and J. A. Burns, *Icarus* **74**, 284 (1988).
17. F. Poulet and B. Sicardy, *Bull. Am. Astron. Soc.* **29**, 1001 (1997).
18. Grains larger than 100 μm make a negligible contribution in all except the very flattest size distributions.
19. J. B. Pollack and J. N. Cuzzi, *J. Atmos. Sci.* **37**, 868 (1980).
20. J. N. Cuzzi and R. H. Durisen, *Icarus* **84**, 467 (1990).
21. D. H. Humes, *J. Geophys. Res.* **85**, 5841 (1980).
22. J. N. Cuzzi and P. R. Estrada, *Icarus* **132**, 1 (1998).
23. L. R. Doyle, L. Dones, J. N. Cuzzi, *ibid.* **80**, 104 (1989).
24. R. H. Durisen *et al.*, *ibid.* **124**, 220 (1996).
25. G. E. Morfill, H. Fechtig, E. Grün, C. K. Goertz, *ibid.* **55**, 439 (1983).
26. D. T. Hall, P. D. Feldman, J. B. Holberg, M. A. McGrath, *Science* **272**, 516 (1996).
27. E. Grün, G. E. Morfill, R. J. Terrile, T. V. Johnson, G. Schwehm, *Icarus* **54**, 227 (1983).
28. C. K. Goertz and G. E. Morfill, *ibid.* **53**, 219 (1983).
29. G. E. Morfill, E. Grün, C. K. Goertz, T. V. Johnson, *ibid.*, p. 230.
30. M. Tagger, R. N. Henriksen, R. Pellat, *ibid.* **91**, 297 (1991).
31. J. R. Hill and D. A. Mendis, *J. Geophys. Res.* **87**, 7413 (1982).
32. E. Grün, G. W. Garneau, R. J. Terrile, T. V. Johnson, G. E. Morfill, *Adv. Space Res.* **4** (no. 4), 143 (1984).

33. I thank J. Cuzzi, L. Dones, and J. Lissauer for helpful discussions and comments and E. Duxbury and A. Wasserman of the Planetary Data System Imaging Node for extensive help with obtaining the data. Supported by NASA's Planetary Geology and Geophysics program through grant 344-30-51-05.

20 July 1998; accepted 7 October 1998

Neptune's Partial Rings: Action of Galatea on Self-Gravitating Arc Particles

Heikki Salo* and Jyrki Hänninen

Numerical simulations of Neptune's arcs show that self-gravity between macroscopic arc particles can prevent interparticle impacts and thereby stabilize their resonant confinement by Galatea, a satellite of Neptune. Stable subkilometer arc particles provide a source for replenishing the observed dust and explain the clumpy substructure seen in arcs. A few confining kilometer-sized particles between the major arc components can account for the observed arc widths spanning several resonance sites. The modeled distribution of dust is consistent with observations and helps to explain how embedded satellites may affect the structure and evolution of planetary ring systems.

Voyager 2 detected partial rings (arcs) around Neptune in August 1989 (*1*), confirming earlier Earth-based stellar occultation observations (*2*). The observed dusty material is concentrated in four 4°- to 10°-wide arcs (*3*), with a total azimuthal span of 40°. The arcs, with optical depths of about $\tau_a \sim 0.1$ are embedded in a diffuse Adams ring ($\tau_d \sim 0.003$) at a mean distance $a = 62{,}932$ km from Neptune. Arcs contain unresolved clumps of bright objects, containing dust (radius $r < 100$ μm) and larger ($r > 100$ μm) particles (*4*). The dust contributes 50 to 95% of the total τ of the arcs (*5*). The radial width of the arcs is $W_a \approx 15$ km, and they show radial distortion with amplitudes of about 30 km, while for the diffuse ring, $W_d \approx 50$ km.

The geometry and kinematic behavior of the arcs was explained by the resonant forcing due to the satellite Galatea, which orbits about 980 km inside the arcs (*6*). Its 42:43 corotation-inclination resonance (CIR) generates $2m_c = 86$ evenly spaced corotation sites around the ring (*7*). The guiding centers (mean positions) of particles librate around these sites, which correspond to local maxima in the gravitational potential (*8*). The nearby (~1.5 km inward of CIR) 42:43 outer Lindblad resonance (OLR) forces particles to have closed orbits in the reference frame of Galatea and is responsible for the observed radial distortions of the arcs.

Strictly speaking, the resonance model is only valid for macroscopic particles. Besides Galatea's perturbations dust grains are affected by radiation forces. The grains with $r <$ 100 μm are removed from CIR sites and possibly also from the diffuse ring in less than 100 years, because of solar radiation pressure (*9*). However, larger grains in CIR sites are shielded from the secular effects of Poynting-Robertson (PR) drag, whereas outside the sites, PR drag will drive them toward OLR which will increase their eccentricities (*9*). For example, icy grains will reach $e \sim W_d/a$, corresponding to the width of Adams ring, on time scales $T_{\text{Adams}} \sim 3 \times 10^3$ (r/100 μm) years. These short time scales suggest that the dust observed in CIR sites, and in the diffuse ring, is continuously replenished by impacts between macroscopic arc particles, which are unaffected by radiation forces. This scenario does not stabilize the arcs, however,

Division of Astronomy, Department of Physical Sciences, University of Oulu, FIN-90570 Oulu, Finland.

*To whom correspondence should be addressed. E-mail: hsalo@sun3.oulu.fi

because impacts between macroscopic arc particles in turn destroy their resonance locking with Galatea. Namely, the width of the CIR zone $\Delta a \approx 0.3$ km $\ll W_a$, which indicates large eccentricity gradients in the arcs and consequently large relative velocities, $v_{coll} \approx 1$ m/s between particles. Our previous numerical simulations showed that typical post-collisional tangential velocity increments $\delta v_{tan} \gg \delta v_{min} \approx 2$ cm/s, which is the minimum required for an escape from a CIR site (*10*). The time scale for destabilization of the large arc particles is thus comparable to the average time between their mutual impacts, $T_{coll} \approx 20\ T_{per}/\tau_m$, where τ_m is the optical depth of macroscopic particles and $T_{per} \approx 0.001$ years is the orbital period. Even if $\tau_m \ll \tau_a$, T_{coll} is only a few years. Once free from resonance locking, macroscopic particles and most of the impact debris leave the original CIR site on time scales comparable to the CIR libration period, about $T_{site} \simeq 3000\ T_{per}$. Without additional confinement the time scale for complete azimuthal randomization is only about an order of magnitude larger than T_{site}.

A model consistent with the above considerations would assume a single large particle (with radius $R_L \sim 0.1$ to 1 km) in each site occupied by arcs. During their radial excursions they would be hit by dust and small meter-sized particles from the diffuse ring. These impacts would not endanger the stability of the large arc particle, but would create dust debris that migrates from the CIR sites to the diffuse ring, and then either disperses due to PR drag or reaccretes on the large arc particles. However, this model does not explain why the main arc components have widths spanning several CIR sites. It also fails to account for the overall density contrast between the diffuse ring and the arcs. Namely, by assuming a steady state in the production of dust debris in arc sites and the dispersal of diffuse ring, we obtained $\tau_a/\tau_d \approx T_{site}/T_{Adams} W_d/W_a\ 360°/4.18° < 1$ for $r > 100$ μm. Rapid reaccretion of dust back from the diffuse ring to arc particles would enhance the density contrast. However, our calculations indicate that the typical reaccretion time scale $T_{capt} \approx 3 \times 10^3$ (1 km/R_L)^2 years is comparable to the above estimate for T_{Adams} if $R_L \approx 1$ km. Thus, reaccretion cannot solve the contrast problem, although dust recycling would lengthen the total lifetime of the system. Enhancing the contrast requires an additional confining mechanism that will increase the time dust spends in the arc region.

Here, we concentrate on macroscopic particles unaffected by radiation forces. Our treatment is also valid for large dust grains ($r > 100$ μm) for the studied time spans. Self-gravity of individual large arc particles, which has been overlooked in previous treatments, provides a mechanism that can prevent their mutual collisions, and also helps to confine the arc region in general. An important counter-intuitive feature of the orbital dynamics of particles sharing a common mean motion is the apparently repulsive nature of mutual gravity between particles. The motion is at all times dominated by the planet's gravitational field, coupling the changes in mean motion and mean distance from the planet. For example, consider a particle pair where the other particle is momentarily at a slightly smaller mean distance and approaching the outer particle. It gains angular momentum due to the force exerted by the outer one, which in a Keplerian force field implies increase of its mean distance. This prevents the collision by slowing down the inner particle and eventually reversing the roles of inner and outer particle. An approximation for the motion of N co-orbital particles yields (*11, 12*)

$$d(\delta n_i^{sg})/dt = 3n_0^2 \sum_{\substack{j=1 \\ j \neq i}}^{N} \mu_j \sin(\lambda_{ij})\,(8|\sin(\lambda_{ij}/2)|^{-3} - 1),\ i = 1, \ldots N \quad (1)$$

where δn_i^{sg} denotes the deviation of the particle's mean motion from the common mean value n_0, while $\lambda_{ij} = \lambda_i - \lambda_j$, where λ values are the particles' mean longitudes, and μ values denote masses of particles relative to the planet [this expression is accurate to $O(\mu)$]. The second term on the right-hand side follows from the indirect terms due to fixing the center of the coordinate system to the central body. For $N = 2$ particles, $d(\delta n_i)/dt = 0$ for $\lambda_{ij} = 60°$ or 180°: the former corresponds to the stable equilateral solution (*13*), while the latter is unstable. Stable stationary configurations, where particles are concentrated on the same side of the common mean orbit exist for $N \leq 8$ particles (*12*).

To determine how self-gravity between particles locked in Galatea's resonance sites can affect their dynamics, Eq. 1 was combined with the CIR forcing term

$$d(\delta n_i^c)/dt = -6 m_c n_0^2 \epsilon I_m^2 \sin(2 m_c \lambda_i) \quad (2)$$

where λ_i is the deviation from the center of the resonance site, I_m is the relative inclination of Galatea with respect to arcs, and $\varepsilon \approx 3.3 \times 10^{-6}$ is the resonance strength (*9*). Provided that μ_i values are small enough, there exists stationary solutions for which $d(\delta n_i^{sg} + \delta n_i^c)/dt$ vanish simultaneously for all i. Around these relative positions, the motion can be approximated with Eqs. 1 and 2. This predicts: (i) Several particles with

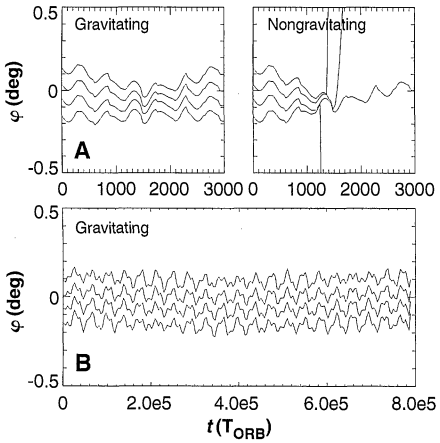

Fig. 1. Numerical integration of four 100-m radii particles located in Galatea's resonance site. The longitude of particles (in a system corotating with the CIR site) is displayed versus time. In (**A**), the gravitating (internal density of particles $\rho = 900$ kg/m^3) and nongravitating ($\rho = 0$) cases are compared; in the latter case, mutual impacts rapidly eject all except one particle from the site. (**B**) demonstrates the long-term stability of the gravitating case. Integrations employed a Runge–Kutta-4 integrator in a rotating cylindrical coordinate system. The orbital elements of arcs and Galatea are the same as in (*10*).

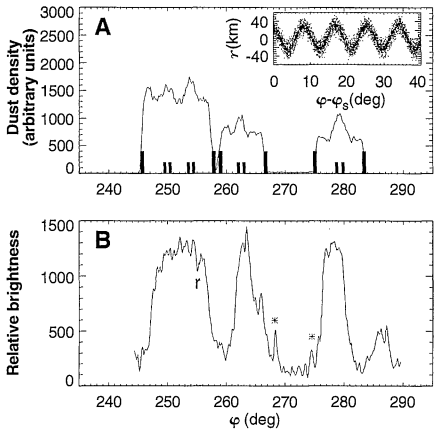

Fig. 2. (**A**) displays a possible schematic configuration of macroscopic particles in Neptune arc sites. Icy particles with $R = 0.1$ and 1 km are assumed, and their locations are chosen in the manner that qualitatively reproduces the three main arcs. For example, the widest arc is confined by two 1-km particles located at resonance sites $3 \times 4.18°$ apart, and the two interior sites are both occupied by a pair of 100-m particles (mean positions are marked by vertical bars). Dust originates from the surfaces of 100-m particles as described in the text. Altogether, 400 dust grains were launched, and their time-averaged distribution in a simulation lasting $10^5\ T_{per}$ is shown. (**B**) [data from (*4*)] displays the observations [symbols denote locations of uncompletely removed camera reseau (r) and background stars (asterisks)]. Note that in our model, the intepretation of the correspondence between ring edges and CIR sites differs (*16*) from that in (*6*). The insert in (A) displays dust particle radial excursions in a coordinate system corotating with Galatea.

$R < R_{cr}$ can remain resonance-locked in a single site on noncolliding orbits. For $N = 2$ similar-sized icy particles, $R_{cr} \simeq 2$ km, while for $N = 10$, $R_{cr} \simeq 0.5$ km. For a large particle to allow small test particles in the same site, $R_{cr} \simeq 1.4$ km. Numerical integrations of full dynamical equations confirm these qualitative predictions (Fig. 1), although because of OLR perturbations, the actual R_{cr}'s are about 50% smaller. These estimates assume (*10*) $I_m = 0.0495°$; for other values of I_m, $R_{cr} \propto I_m^{2/3}$. (ii) Adjacent resonance sites can hold particles: our simplified treatment predicts that $N = 2$ similar-sized particles, started $k \times 4.18°$ apart, remain resonance locked with Galatea, if $R < R_{cr} = 3.2$, 4.8, and 6.1 km for $k = 1$, 2, and 3, respectively. Full integrations indicate about 15% smaller limits for R_{cr}. The resonance locking survives even if the large particles librate (<1°) around the site centers. (iii) Particles escaping a resonance site can stay confined by massive particles occupying adjacent sites, as the tangential velocity increments of escaped particles are reverted in close gravitational encounters with massive particles. Formally, Eq. 1 does not give any upper limit for the maximal approach velocity that can be reverted. However, Eq. 1 breaks down when the implied minimum longitude of approach becomes comparable to $b \times \phi_{HILL}$, where $\phi_{HILL} = (\mu/3)^{1/3}$ denotes the Hill sphere of the massive particle; for closer encounters, the approaching particle can cross the longitude of the large particle and be ejected. Our integrations show that $b > 10$ provides stability in the case of several tens of close encounters with massive particles. This corresponds to maximal $\delta v_{tan} \simeq 10$ (R/1 km) cm/s.

On the basis of the above consideration, we propose the following schematic dynamical configuration for Neptune's arcs: (i) Most of the sites in the arc region contain macroscopic particles in the radius range 0.1 to 1 km. A given site can either hold several subkilometer particles in noncolliding orbits or just a single particle with $R \approx 1$ km. (ii) Dust is produced in impacts of meter-sized stray particles on the arc particles. The stray particles are distributed throughout the diffuse Adams ring. Typical impact velocities are of the order of a few meters per second, large enough to produce dust debris (*14*). Postcollisional velocities of the dust are typically 10 cm/s, while the meter-sized bodies could rebound from the collisions with larger velocity. (iii) Primary sources of observed dust are the subkilometer particles, located in the sites on arc segments. In impacts with kilometer-sized particles, most of the debris returns to their surfaces, because of larger escape velocity [$v_{esc} \approx 70$ (R/1 km) cm/s]. The main role of kilometer-sized particles is to separate different arc segments, by partially confining the dust escaping from the arcs. (iv) The clumpy substructure seen in some arcs results from the dust ejected from several subkilometer particles sharing the same site. The observed spacing ~0.5° is consistent with source particles in the radius range of a few hundred meters.

Our model for dust production assumes that the macroscopic arc particles are covered by dust. The stray particles, with nominal radii of 1 m, are assumed to move in circular orbits. The relative impact velocity and angle depend on the phase of the arc particle, v_{coll} ranging from 2 to 6 m/s. The Holsapple-Schmidt scaling relationship with empirical data for low-speed impacts on pumice targets is used to calculate the dust ejection velocities (*15*). With these assumptions, most of the dust debris resulting in impacts with 100-m particles leaves the original site with velocities <10 cm/s. However, because of kilometer-sized particles, this debris remains confined to the arc region. The model dust distribution is similar to the observed distribution of dust (Fig. 2). Moreover, although the dust particles are not confined to single sites but bounce between kilometer-sized particles, they still show the OLR signature as required by the observations.

Over longer time scales of $T_{arcs} \simeq 10^3$ years, a typical dust particle escapes from the arc region to the diffuse ring by repeated encounters with kilometer-sized particles. With the previous estimate for T_{Adams}, this leads to $\tau_a/\tau_d \approx T_{arcs}/T_{Adams}\, W_d/W_a\, 360°/40° \approx 10$. Inclusion of the reaccretion on large particles (for the configuration of Fig. 2, $T_{capt} \approx 500$ years) increases the density contrast by a factor of ~5. These estimates are consistent with the observed $\tau_a/\tau_d \approx 30$. Note, however that our estimate of T_{arcs} ignores radiation forces and thus refers only to the largest dust grains ($r > 100$ μm). The implied overall density contrast could be smaller, if smaller dust grains are more evenly distributed. Indeed, observations (*2*) suggest that large grains ($r > 100$ μm) are overabundant in the arcs as compared to the diffuse ring. However, the confinement could be made more effective by increasing the sizes of the particles separating the arc segments or by reducing the dust ejection velocities (*15*). Our confinement mechanism due to kilometer-sized particles works even if I_m is smaller than the nominal value of 0.0495°.

The model we propose for the distribution of macroscopic particles in Neptune ring arcs is stable against particle impacts. Self-gravity between individual arc particles prevents impacts between subkilometer particles sharing a common site and offers an explanation for the bright clumps in the arcs. Dust ejected from these particles, although readily leaving the original site, becomes confined by the gravity of additional kilometer-sized particles separating different arcs. Because these confining particles are not necessarily located on the nearest adjacent sites, arcs can extend over several site widths. The long time scale for dust to remain in the arc region causes the observed density contrast between arc and diffuse ring. Although we offer a plausible steady-state model for the current arc system, the origin of the proposed distribution of macroscopic particles is open. However, it seems likely that many possible processes (for example satellite disruption or accretion near the Roche zone) responsible for the formation of the resonance-locked ring would involve a wide distribution of particle sizes. Interaction between large (for instance, 100 m to 1 km) and the more abundant small (for instance, meter-sized) particles could stabilize some large particles into resonance sites at the expense of smaller ones, which would end up in the diffuse ring or be ejected from the system.

References and Notes

1. B. A. Smith *et al.*, *Science* **246**, 1422 (1989).
2. B. Sicardy, F. Roques, A. Brahic, *Icarus* **89**, 220 (1991).
3. The three main arc segments, embedded in the Neptune's outermost (Adams) ring are named Fraternité, Egalité, and Liberté, from trailing arc to leading arc, respectively. The fourth arc segment, Courage, is less conspicuous than the others.
4. C. Porco, P. Nicholson, J. Cuzzi, J. Lissauer, L. Esposito, in *Neptune and Triton*, D. Cruikshank, Ed. (Univ. of Arizona Press, Tucson, AZ, 1995), pp. 703–804.
5. C. Ferrari and A. Brahic, *Icarus* **111**, 193 (1994).
6. C. C. Porco, *Science* **253**, 995 (1991).
7. The corotation-inclination resonance (CIR) condition, $m_c n = (m_c - 1)n_s + \dot{\Omega}_s$, is fulfilled when the mean motion n of a particle is commensurable with the vertical frequency of the satellite (n_s and $\dot{\Omega}_s$ are a satellite's mean motion and nodal precession rate, respectively). The outer Lindblad resonance condition, $m_L n_s = (m_L + 1)n - \dot{\varpi}$, requires commensurability between a particle's radial frequency and a satellite's mean motion ($\dot{\varpi}$ denotes a particle's apsidal precession rate). For the Neptune arcs, $m_c = 43$ and $m_L = 42$, and both resonances are labeled as 42:43 resonances. There is a shift of ~1.5 km in the CIR and OLR radii, which is due to the oblateness of Neptune. The time-averaged motion of an arc particle fulfills both of these conditions.
8. P. Goldreich, S. Tremaine, N. Borderies, *Astron. J.* **92**, 490 (1986). The nearby OLR stabilizes infinitesimal oscillations around a CIR site, although this represents a local potential maximum.
9. D. W. Foryta and B. Sicardy, *Icarus* **123**, 129 (1996).
10. J. Hänninen and C. Porco, *ibid.* **126**, 1 (1997). These simulations studied the collisional evolution of macroscopic arc particles, but did not include their mutual self-gravity.
11. C. F. Yoder, G. Colombo, S. P. Synnot, K. A. Yoder, *ibid.* **53**, 431 (1983).
12. H. Salo and C. F. Yoder, *Astron. Astrophys.* **205**, 309 (1988).
13. The equilateral solution of three-body motion was found by Lagrange in 1772.
14. J. Colwell and L. Esposito, *Geophys. Res. Lett.* **17**, 1741 (1990).
15. W. Hartmann [*Icarus* **63**, 69 (1985)] found the relative kinetic energy for the ejecta to be $E_{ejecta}/E_{impact} = 1 \times 10^{-3}$. We have taken a conservative view and adopted a 10-fold value, which will increase the amount of dust escaping from arcs.
16. In the kinematical model of Porco (*6*), the arcs are centered on CIR sites, whereas in our model, the arcs are bounded by massive particles librating at site centers. The difference is one-half of the site width or 2.1°, which is below current observational uncertainty.

17. This research was supported by the Academy of Finland.

7 July 1998; accepted 6 October 1998